

# Supportive Information (SI) for “A unified theory on gravity current, interfacial and unsaturated flows in heterogeneous porous layers”

Zhong Zheng<sup>1,2,\*1</sup>

<sup>1</sup>State Key Laboratory of Ocean Engineering, School of Ocean and Civil Engineering, Shanghai Jiao Tong University, Shanghai 200240, PR China

<sup>2</sup>MOE Key Laboratory of Hydrodynamics, School of Ocean and Civil Engineering, Shanghai Jiao Tong University, Shanghai 200240, PR China

\*Corresponding author. E-mail: [zzheng@alumni.princeton.edu](mailto:zzheng@alumni.princeton.edu); [zhongzheng@sjtu.edu.cn](mailto:zhongzheng@sjtu.edu.cn)

**Received:** XX 202X; **Revised:** XX XX 202X; **Accepted:** XX XX 202X

**Keywords:** Wetting and Capillary Effects; Interfacial and Unsaturated Flow; Heterogeneity

## 1. Introduction

We provide additional derivations, calculations and remarks here as supportive information (SI) for the maintext entitled “A unified theory on gravity current, interfacial and unsaturated flows in heterogeneous porous layers”. The model problem is sketched in figure 1. The SI includes two parts: In §2, we provide additional numerical results on the profile shape evolution that demonstrates the time transition from early-time unconfined to late-time confined self-similar solutions in the significantly unsaturated flow regime. In §3, we briefly describe a finite volume scheme that has been employed to solve the time evolution system of one-dimensional gravity current, interfacial and unsaturated flows.

## 2. Time Transition

To demonstrate the time transition in the significantly unsaturated flow regime ( $B \ll 1$ ), we numerically solve the time-dependent PDE subject to appropriate IBCs, given by

$$\frac{\partial \bar{I}_s(\bar{h})}{\partial \bar{t}} + \frac{\partial}{\partial \bar{x}} \left[ \frac{N \bar{I}_n(\bar{h})}{N \bar{I}_n(\bar{h}) + \bar{I}_w(\bar{h})} \right] - \frac{\partial}{\partial \bar{x}} \left[ \frac{\bar{I}_n(\bar{h}) \bar{I}_w(\bar{h})}{N \bar{I}_n(\bar{h}) + \bar{I}_w(\bar{h})} \frac{\partial \bar{h}}{\partial \bar{x}} \right] = 0, \quad (1)$$

and

$$\bar{I}_s(\bar{h}) \sim \frac{B \Lambda \bar{h}^{2\delta/n+\delta+2}}{(2\delta/n + \delta + 1)(2\delta/n + \delta + 2)}, \quad (2a)$$

$$\bar{I}_n(\bar{h}) \sim \frac{2B^2 \Lambda^2 \bar{h}^{4\delta+3}}{(4\delta + 1)(4\delta + 2)(4\delta + 3)}, \quad (2b)$$

$$\bar{I}_w(\bar{h}) \sim \frac{1}{2\delta + 1} - \frac{2B \Lambda \bar{h}^{3\delta+2}}{(3\delta + 1)(3\delta + 2)} + \frac{2B^2 \Lambda^2 \bar{h}^{4\delta+3}}{(4\delta + 1)(4\delta + 2)(4\delta + 3)}, \quad (2c)$$

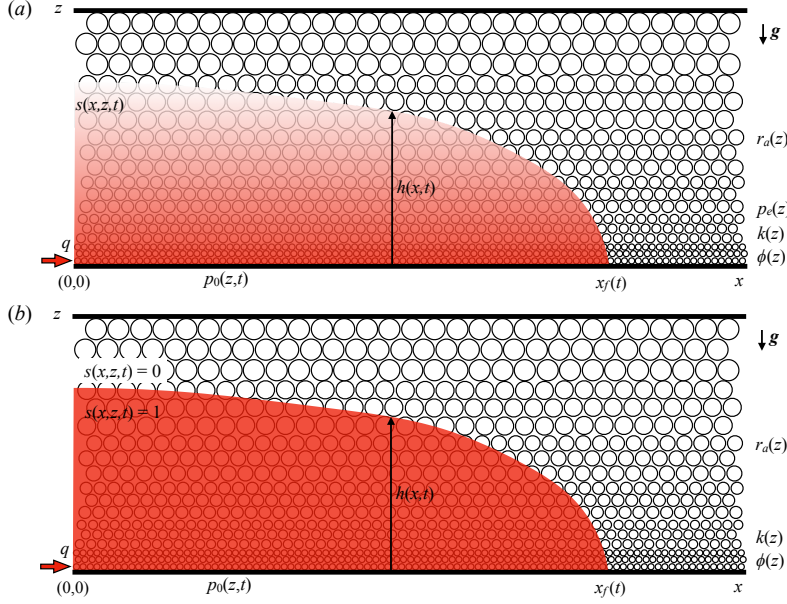


**Figure 1.** A schematic of an unsaturated flow in (a) and sharp-interface flow in (b) in a porous layer with vertical heterogeneity. The average pore radius  $r_a(z)$  varies vertically, so as the intrinsic permeability  $k(z)$ , porosity  $\phi(z)$ , and capillary entry pressure  $p_e(z) \equiv \gamma \cos \theta / r_a(z)$ . The injection rate, effective saturation, and outer envelope of the invading fluid are denoted by  $q$ ,  $s(x, z, t)$ , and  $h(x, t)$ , respectively, and the location of the propagating front is denoted by  $x_f(t)$ .

subject to

$$\bar{h}(\bar{x}, 0) = 0, \quad (3a)$$

$$\bar{h}(\bar{x}_f(\bar{t}), \bar{t}) = 0, \quad (3b)$$

$$\left[ \frac{N \bar{I}_n(\bar{h})}{N \bar{I}_n(\bar{h}) + \bar{I}_w(\bar{h})} - \frac{\bar{I}_n(\bar{h}) \bar{I}_w(\bar{h})}{N \bar{I}_n(\bar{h}) + \bar{I}_w(\bar{h})} \frac{\partial \bar{h}}{\partial \bar{x}} \right] \bigg|_{\bar{x}=0} = 1. \quad (3c)$$

A shock-capturing finite-volume scheme was implemented to solve the nonlinear advective-diffusive equation, following a series of earlier studies (e.g., [Zheng et al., 2015](#); [Guo et al., 2016](#); [Hinton & Woods, 2018](#)). A brief description of the scheme is provided later in §3, which is central difference in space and explicit in time. The grid size was made small enough such that no significant difference was observed for both the frontal location and interface shape, when the number of grids increases. In particular, for the numerical solutions shown here, it is ensured that the difference for the frontal location  $\bar{x}_f(\bar{t})$  is within 1% when the number of grids doubles.

In the example calculations here, we impose  $\{\delta, n, N, B\Lambda\} = \{1, 2, 8 \times 10^4, 10^{-1}\}$  in figure 2 and  $\{\delta, n, N, B\Lambda\} = \{1, 2, 2, 10^{-1}\}$  in figure 3. It is illustrated in figure 2 that a time transition from an early-time nonlinear diffusive solution (for a capillary film) towards a late-time compound-wave solution (for unsaturated flows) appears for sufficiently large viscosity ratio ( $N = 8 \times 10^4$ ). It is also of interest to note that relatively more significant difference appears in figure 2b between the compound-wave and rescaled PDE solutions in two regions as  $\bar{x} \rightarrow 0^+$  and  $\bar{x} \rightarrow \bar{x}_f(\bar{t})^-$ . This is due to the singular perturbation effects of the diffusive term in PDE (1a). In contrast, for smaller viscosity ratio ( $N = 2$ ), following the same early-time nonlinear diffusive behaviour in figure 2a (for  $N = 8 \times 10^4$ ), a time transition towards a late-time shock solution appears in figure 3.

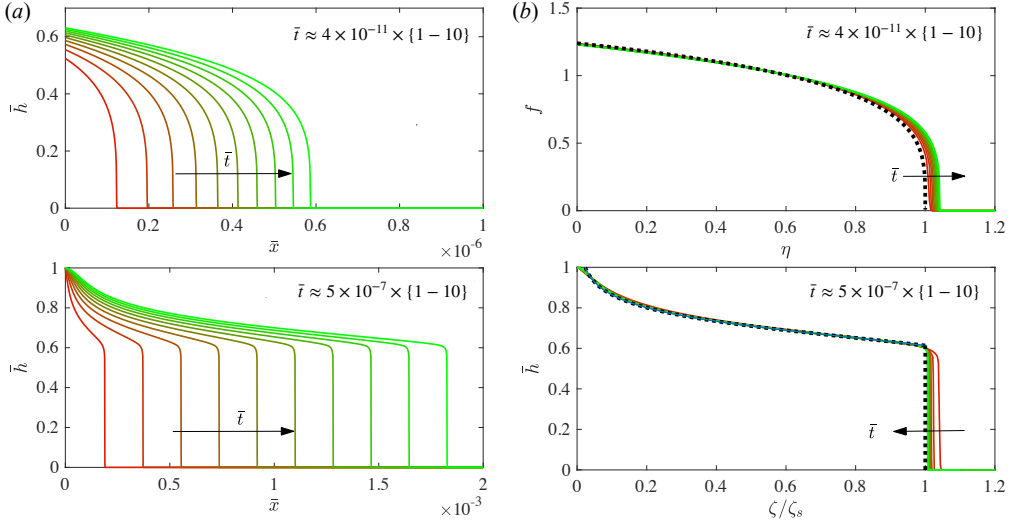


**Figure 2.** Time evolution of  $\bar{h}(\bar{x}, \bar{t})$ , shape of the outer envelope of the invading fluid, in the significantly unsaturated flow regime ( $B \ll 1$ ), imposing  $\{\delta, n, N, B\Lambda\} = \{1, 2, 8 \times 10^4, 10^{-1}\}$ : (a) Raw numerical solutions of (1) and (2) at both the early and late times, (b) Rescaled numerical solutions, and a comparison with the self-similar solutions at both the early and late times, shown as the dashed curves. The location and height of the inserted shock front is  $(\zeta_s, \bar{h}_s) \approx (363, 0.614)$  for the compound-wave solution at late times.

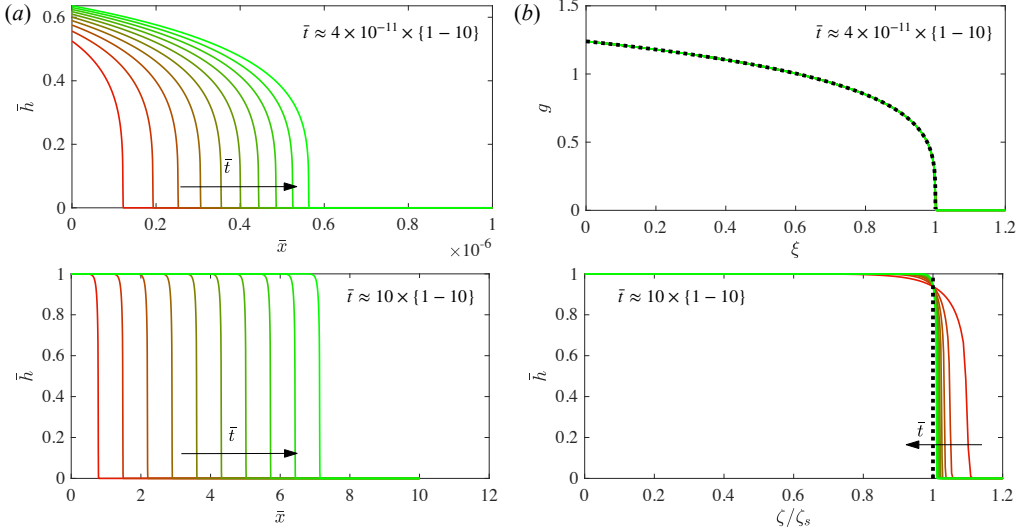


**Figure 3.** Time evolution of  $\bar{h}(\bar{x}, \bar{t})$ , shape of the outer envelope of the invading fluid, in the significantly unsaturated flow regime ( $B \ll 1$ ), imposing  $\{\delta, n, N, B\Lambda\} = \{1, 2, 2, 10^{-1}\}$ : (a) Raw numerical solutions of (1) and (2) at both the early and late times, (b) Rescaled numerical solutions, and a comparison with the self-similar solutions at both the early and late times, shown as the dashed curves. The location of the shock is  $\zeta_s \approx 0.0706$  at late times.

### 3. Numerical Scheme

We provide a brief description here on a shock-capturing finite-volume scheme, employed to solve PDE (1) for the time evolution of the interface shape  $\bar{h}(\bar{x}, \bar{t})$  in this study. Similar schemes have been used in a series of earlier studies that are related to the nonlinear advective-diffusive PDEs (e.g., [Zheng et al., 2015](#); [Guo et al., 2016](#); [Hinton & Woods, 2018](#)). For significantly unsaturated flows, the saturation and permeability integrals  $\bar{I}_s(\bar{h})$ ,  $\bar{I}_n(\bar{h})$  and  $\bar{I}_w(\bar{h})$  in PDE (1) are approximated by (2), while for sharp-interface flows, the integrals are approximated differently. These explicit expressions allow us to construct the numerical scheme conveniently in each of the asymptotic regimes.

We start by defining a dimensionless flux  $\bar{Q}(\bar{x}, \bar{t})$ , such that

$$\frac{\partial \bar{I}_s}{\partial \bar{t}} = \frac{\partial \bar{Q}}{\partial \bar{x}}, \quad \text{where} \quad \bar{Q} \equiv -\frac{N\bar{I}_n}{N\bar{I}_n + \bar{I}_w} + \frac{\bar{I}_n\bar{I}_w}{N\bar{I}_n + \bar{I}_w} \frac{\partial \bar{h}}{\partial \bar{x}}. \quad (4)$$

This is a common treatment of a finite-volume scheme for a PDE of the evolution type. The numerical scheme is to provide solutions for  $\bar{h}_j^i \equiv \bar{h}(\bar{x}, \bar{t})$ , where  $\bar{x} = (j - 1/2)\Delta\bar{x}$  and  $\bar{t} = (i - 1)\Delta\bar{t}$ . Specifically,  $i = 1, 2, \dots$  denotes the time steps and  $j = 1, 2, 3, \dots, J - 1, J$  denotes the space grids. The domain is defined within  $\bar{x} \in [0, L]$ , so  $\Delta\bar{x} = L/(J - 1/2)$ . The flux  $\bar{Q}_{j+1/2}^i$  is defined between two space grids  $j$  and  $j + 1$  with  $j = 1, 2, \dots, J - 1$ , and at the boundary of the domain  $\bar{Q}_{1/2} = 1$  and  $\bar{Q}_{J+1/2} = 0$  are imposed based on the flux and frontal boundary conditions at  $\bar{x} = 0$  and  $\bar{x} = L$ , respectively. Then, PDE (4) can be rewritten as

$$\bar{I}_{s,j}^{i+1} = \bar{I}_{s,j}^i + \frac{\Delta\bar{t}}{\Delta\bar{x}} \left( \bar{Q}_{j+1/2}^i - \bar{Q}_{j-1/2}^i \right), \quad (5)$$

for  $j = 1, 2, 3, \dots, J - 1, J$ , where

$$\bar{Q}_{j+1/2}^i = -\frac{N\bar{I}_{n,j+1/2}^i}{N\bar{I}_{n,j+1/2}^i + \bar{I}_{w,j+1/2}^i} + \frac{\bar{I}_{n,j+1/2}^i \bar{I}_{w,j+1/2}^i}{N\bar{I}_{n,j+1/2}^i + \bar{I}_{w,j+1/2}^i} \frac{(\bar{h}_{j+1}^i - \bar{h}_j^i)}{\Delta\bar{x}}, \quad (6)$$

for  $j = 1, 2, \dots, J - 1$ . Forward Euler method has been imposed for the time evolution in (5).

(4) to (6) apply for both the significantly-unsaturated and sharp-interface flow regimes, while the saturation and permeability integrals  $\bar{I}_{s,j}^i$ ,  $\bar{I}_{n,j+1/2}^i$  and  $\bar{I}_{w,j+1/2}^i$  could take different expressions. For example, based on explicit solution (2) for significantly unsaturated flows in porous layers, the integrals are approximated by

$$\bar{I}_{s,j}^i = \frac{B\Lambda}{(\delta + 2\delta/n + 1)(\delta + 2\delta/n + 2)} \left( \bar{h}_j^i \right)^{2\delta/n + \delta + 2}, \quad (7a)$$

$$\bar{I}_{n,j+1/2}^i = \frac{2B^2\Lambda^2}{(4\delta + 1)(4\delta + 2)(4\delta + 3)} \left( \frac{\bar{h}_j^i + \bar{h}_{j+1}^i}{2} \right)^{4\delta + 3}, \quad (7b)$$

$$\bar{I}_{w,j+1/2}^i = \frac{1}{2\delta + 1} - \frac{2B\Lambda}{(3\delta + 1)(3\delta + 2)} \left( \frac{\bar{h}_j^i + \bar{h}_{j+1}^i}{2} \right)^{3\delta + 2} + \frac{2B^2\Lambda^2}{(4\delta + 1)(4\delta + 2)(4\delta + 3)} \left( \frac{\bar{h}_j^i + \bar{h}_{j+1}^i}{2} \right)^{4\delta + 3}. \quad (7c)$$

In contrast, based on explicit solution for sharp-interface flows, the integrals are approximated by

$$\bar{I}_{s,j}^i = \frac{1}{2\delta/n + 1} \left( \bar{h}_j^i \right)^{2\delta/n + 1}, \quad (8a)$$

$$\bar{I}_{n,j+1/2}^i = \frac{1}{2\delta + 1} \left( \frac{\bar{h}_j^i + \bar{h}_{j+1}^i}{2} \right)^{2\delta + 1}, \quad (8b)$$

$$\bar{I}_{w,j+1/2}^i = \frac{1}{2\delta + 1} - \frac{1}{2\delta + 1} \left( \frac{\bar{h}_j^i + \bar{h}_{j+1}^i}{2} \right)^{2\delta + 1}. \quad (8c)$$

We also note that (7a) and (8a) apply at  $j = 1, 2, 3, \dots, J - 1, J$ , while (7b,c) and (8b,c) apply at  $j = 1, 2, 3, \dots, J - 1$ .

We have thus obtained a finite volume scheme for the numerical solution of the shape of the interface  $\bar{h}_j^i$ . Providing an initial condition, e.g.,  $\bar{h}_j^1 = 0$ , we can calculate the time evolution of the interface shape  $\bar{h}_j^i$  at  $i = 2, 3, 4, \dots$  using (5). The scheme is first order in time and second order in space. The time and space steps are chosen to be small enough such that the scheme is stable and no significant difference is observed for both the frontal location and interface shape upon grid refinement. Typical grid number is  $J = O(10^3)$  in this study, and it is ensured that the difference for the frontal location is less than 1% when the grid number doubles.

## References

- GUO, B., ZHENG, Z., CELIA, M.A. & STONE, H.A. 2016 Axisymmetric flows from fluid injection into a confined porous medium. *Phys. Fluids* **28**, 022107.
- HINTON, E.M. & WOODS, A.W. 2018 Buoyancy-driven flow in a confined aquifer with a vertical gradient of permeability. *J. Fluid Mech.* **848**, 411–429.
- ZHENG, Z., GUO, B., CHRISTOV, I.C., CELIA, M.A. & STONE, H.A. 2015 Flow regimes for fluid injection into a confined porous medium. *J. Fluid Mech.* **767**, 881–909.